NASA Technical Memorandum 82963

Turbofan Blade Stresses Induced by the Flow Distortion of a VTOL Inlet at High Angles of Attack

Robert C. Williams, James H. Diedrich, and Robert J. Shaw
Lewis Research Center
Cleveland, Ohio

January 1983

NASA

TURBOFAN BLADE STRESSES INDUCED BY THE FLOW DISTORTION OF A VTOL INLET AT HIGH ANGLES OF ATTACK

Robert C. Williams, James H. Diedrich, and Robert J. Shaw

National Aeronautics and Space Administration
Lewis Research Center
Cleveland, Ohio 44135

SUMMARY

A 51-cm-diameter turbofan with a tilt-nacelle VTOL inlet was tested in the Lewis Research Center's 9- by 15-Ft Low Speed Wind Tunnel at velocities up to 72 m/s and angles of attack up to 120°. Fan-blade vibratory stress levels were investigated over a full aircraft operating range. These stresses were due to inlet air flow distortion resulting from (1) internal flow separation in the inlet, and (2) ingestion of the exterior nacelle wake. Stress levels are presented, along with an estimated safe operating envelope, based on infinite blade fatigue life.

INTRODUCTION

A variety of airframe propulsion configurations are under consideration for future VTOL aircraft. The tilt-nacelle, turbofan-powered airplane shown in figure 1 is one possibility. During cruise, the nacelle axis is nearly parallel to the fuselage axis, but during takeoff and landing, the nacelles are nearly vertical, with the airflow approaching the inlet at an angle of attack occasionally greater than 90°. At high angles of attack, the flow entering the inlet can separate from the inlet inner surface, especially at a reduced engine operating setting. This internal flow separation resembles airfoil stall, and in older literature is referred to as "shroud stall". Proper inlet design (e.g., increased lip thickness) will delay the onset and reduce the severity of flow separation, but may also add to inlet weight and drag. The flow distortion resulting from the flow separation can reduce thrust, cause fan or compressor stall, and excite vibratory blade stresses. Many studies of distortion effects related to stall margin have been made, but few studies of distortion effects on blade stress levels have been made. The stresses may be low at mild distortions, but can lead to blade failure at more severe conditions. Theoretical discussions of the relationship of blade stress to distortion level include references 5 and 6.

This experiment investigated the characteristics and magnitude of the aerodynamically forced blade vibratory stresses at conditions of forward airspeed and angle of attack that typically occur during low-speed operations of tilt-nacelle-type VTOL aircraft. The test results, while unique to the particular combination of inlet and fan, form part of a data base that can be used to confirm analytical procedures intended to predict blade vibration. The aerodynamic performance of the inlet and fan are reported in references 1 to 3 and are not repeated herein.

APPARATUS

Fan

The model fan (fig. 2) has been used for various aerodynamic and acoustic test programs at Lewis. It is 51 cm in diamter, has 15 blades, and has a design pressure ratio of 1.20 at the design rotational speed of 8020 rpm. The unusually low rpm (213 m/s tip speed) was intended to reduce noise. The fan is an adjustable pitch fan, so the blade chord-to-spacing ratio is slightly less than unity to permit 360° rotation of the blades in pitch. Although the model has provisions for pitch change, the pitch was fixed at its design value for the present tests.

The fan blades were made of titanium-6-vanadium-4-aluminum alloy and had a double-circular-arc airfoil section. The blade vibration characteristics are shown on the Campbell diagram of figure 3. Natural vibration frequencies are nearly horizontal lines, with nonrotating values determined by analysis and verified by shake-table testing. The engine order (EO) lines are integral multiples of revolutions per second and are shown by straight lines radiating from the origin. Resonant rotational speeds occur at the intersections of natural frequencies and engine order lines. Because the type of distortion usually observed in the present tests is a nonsinusodial, one-per-revolution excitation, harmonic excitation can make resonant speed a potential condition of high amplitude vibration. Rotating stall, partial stall on the blades, or random turbulence may also result in high stresses at speeds that do not correspond to resonant or integral engine order conditions. The natural frequency at the first bending mode is high enough to permit first bending engine order 1 and 2 (EO 1 and EO 2) resonant speeds that are well above the fan design speed, EO 3 is slightly above design speed. The torsional frequency is quite high, so only EO 8 and above (8 or more torsional vibrations per revolution) are possible. The high torsional frequency makes coupled torsion-bending vibration unlikely.

The stator consisted of 25 blades mounted with the stator leading edge one tip chord downstream of the rotor trailing edge. This large axial spacing was designed to reduce noise.

The fan was driven by a four-stage, axial-flow, high-pressure-heated-air turbine which could develop 900 kW and was capable of driving the fan to rotational speeds of over 9000 rpm, which is 125 percent of the design speed.

Inlet

A schematic of the inlet design is shown in figure 4. The inlet, designed by the Boeing Corporation specifically for tilting-nacelle VTOL application, is asymmetric, with its lower lip thicker than the upper lip. Both internal and external cross sections are circular, but the centers of the cross sections do not coincide. Consult references 1 and 2 for further details of inlet design and aerodynamic performance.

Wind Tunnel and Model Installation

The test facility used was the Lewis 9- by 15-Ft Low Speed Wind Tunnel, which is located in the return leg of the 8- by 6-Ft Supersonic Wind Tunnel. (See fig. 5 and ref. 4 for additional details). The fan-nacelle model installed in the wind tunnel is shown in figure 6. Angle of attack is varied by means of a motor-driven, vertical-axis turntable.

BLADE-STRESS INSTRUMENTATION AND DATA ACQUISITION

Strain gages were located at the root of three fan blades on the suction or convex surface at the midchord position. One gage was used for all recorded and presented vibration data; the other gages generally agreed with the data for the recorded gage. A rotary transformer and related electronics were used to transmit the stress signals from the rotating fan blades. The system for obtaining and recording the strain data is shown in figure 7. The raw signal was recorded on magnetic tape and simultaneously sent to signal analyzers for two types of on-line displays: (1) carpet plots, and (2) stress-amplitude-versus-fan-rotational-speed plots.

Carpet Plots

As illustrated in figure 8, carpet plots are on-line cathode-ray-tube displays that present three variables: frequency, amplitude, and fan rotational speed. These displays were used to monitor and record blade vibration at all frequencies, including unexpected frequencies, such as possible coupled modes. A hard copy printer made permanent records available from the cathode-ray-tube display.

Amplitude Versus RPM Plots

Figure 9 is a sample plot of vibratory stress versus fan rotational speed. Stress amplitude is in terms of percentage of allowable stress, which was obtained by methods summarized in the appendix. The plot gives excellent amplitude information and is restricted to a single frequency by a narrow pass filter (1/3 octave), eliminating all vibration modes except for the first bending mode at 400 Hz. Since the raw signal was recorded on magnetic tape, these plots were available for any other frequency by simply changing filter center frequency before a playback.

TEST PROCEDURES

In order to gather aerodynamic data and to document the extent and intensity of distortion related to separated flow, the inlet was first tested with a full set of instrumentation rakes inside the inlet. These rakes consisted of boundary layer rakes, as well as a set of six equally spaced total-pressure rakes just ahead of the fan. Fan speed was controlled by the model operator, with many stops at set-point conditions while scanning pressure devices recorded all relevant steady-state aerodynamic data.

Blade stresses were monitored during the above aerodynamic testing of the inlet, this served as a safety survey. The stress data, however, were not used, since the presence of the rakes was expected to influence the blade vibration levels. The tests were repeated with a "clean" (no instrumentation rakes) inlet to obtain stress data for this report. An electronic ramp generator controlled fan speed, providing a smooth increase from 1000 to 9000 rpm, then back to 1000 rpm, over a 3 minute period. Both the increasing fan speed and decreasing fan speed stress values were recorded, which served to document stress repeatability and occasional hysteresis, in which inlet flow attachment with increasing fan speed occurred at a higher fan speed than flow separation with decreasing fan speed.

The rpm acceleration or deceleration rate of approximately 5300 rpm per minute was chosen as a compromise between perfect repeatability and excessive testing time. The use of the ramp generator produced excellent plot repeatability, and in this respect was far superior to manual speed control.

The fan-speed excursions described above are shown graphically in figure 10 in relationship to the flow separation characteristics of the inlet. Each fan-speed excursion at a given angle of attack started with separated inlet flow, with eventual attachment as fan speed increased. Decreasing fan speed resulted in the reverse process, attached flow proceeding to separated. After completing tests at one angle of attack, a higher angle of attack was than chosen for the next fan-speed excursion. Testing was halted at the discretion of the test conductor whenever the trend of the stress data suggested entry into an "unsafe testing region" (as shown in fig. 10).

RESULTS AND DISCUSSION

Effect of Inlet Rakes

A short test documented the effect of inlet rakes on blade vibration, the results are shown in figure 11. The six equally spaced rakes caused a slightly higher amplitude stress peak at integral EO 6 (six flatwise bending vibration cycles per revolution), as anticipated, at 3800 rpm. No effect was noted at other rotational speeds. Low-level stresses at resonant rotational speeds were always present, as can be seen in both parts of figure 11. These stresses are ascribed to random tunnel turbulence, since they were present even at zero angle of attack. All data presented in subsequent sections of this report were taken with the inlet rakes removed.

Vibration Modes

All on-line carpet plots were similar to figure 8, as no vibration modes, other than first flatwise bending, occurred during the test. Equipment and procedures had been prepared to document many vibration modes, but the presence of a solitary mode, at approximately 400 Hz, greatly simplified the data analysis and discussion. Because of this, the numerous carpet plots recorded at various fixed conditions of tunnel airspeed and angle of attack are not presented, since amplitude information is more easily read from the plots similar to figure 9.

Typical Stress Characteristics

Before examining the overall data, a typical plot will be examined to explain its features in terms of blade vibratory characteristics and inlet aerodynamics. Figure 12 presents data taken at a free-stream velocity of 38.6 m/s and 90° angle of attack. This particular plot illustrates the features to be seen in most of the other plots and will now be discussed in detail.

Along the abscissa, a scale of integral engine order corresponding to resonant speeds of the first flatwise bending mode of vibration (~ 400 Hz, and designated by EO) has been added. These values were determined from the Campbell diagram of figure 3. In general, local stress peaks occurred at the integral engine orders. If the distortion approaching the fan was constant, one would expect the stresses to increase with fan speed. The stress values dropped, however, due to the lower distortion generated by the inlet at the higher speeds.

Consider now the variation of stress with increasing fan speed. The stresses were low from 1000 to 2700 rpm, where distortion is low because of the internal flow separation around the entire inlet circumference. At about 2800 rpm the leeward lip flow attached, but the windward lip flow remained separated. This occurrence resulted in a one-per-revolution distorted fan flow, and the stresses rose at both integral and nonintegral engine orders. The stresses increased until inlet windward lip flow attachment occurred at 3600 rpm when stress began to fall. The next lower engine order, EO 5, at 4600 rpm was still high. This stress peak was attributed to windward side diffuser flow separation. The separation traversed toward the fan until the diffuser flow was fully attached at about 5500 rpm. Even after the boundary layer was fully attached, the layer was still of nonuni- form thickness circumferentially due to the different longitudinal velocity histories the boundary layer "saw" about the inlet. This effect, as well as random turbulence could have caused the low level stresses at EO 4 and EO 3.

Detailed Stress Characteristics

The primary test results are displayed in figures 13(a) to (f) at free-stream velocity from 30/8 to 72.0 m/s. Trend analysis is facilitated by the composite layout of the plots. Angle of attack increases at constant airspeed in the columns, while tunnel airspeed increases at constant angle of attack in the rows. Each plot, as mentioned previously, uses percentage of allowable stress as the y-axis, with fan rotational speed in rpm as the x-axis.

The general trend of stress induced by inlet flow separation is apparent upon examining figure 13 as a whole. Flow attachment and separation generally occurred at ever-increasing fan rotational speed as functions of increasing airspeed and angle of attack. At the higher airspeeds, stress increased rapidly with angle of attack. Additional details of this effect are shown in figure 14, which shows data at smaller angle of attack increments.

An important and unexpected blade stress, apparently not related to inlet flow separation, was noted. Returning to figure 13(a), one can see that stress rose dramatically at 8200 rpm as angle of attack increased from 100° to 120°. Trends evident in these data also show that inlet flow separation did not occur above 5000 rpm at this low airspeed. Note also that the stress at 8200 rpm, 110° angle of attack, dropped in amplitude as airspeed increased from 30.8 to 38.6 m/s (figs. 13). The flow distortion pattern at the fan face responsible for this stress condition is shown in figure 15(a), and the separated lower lip distortion pattern is shown in figure 15(b). A very thick boundary layer is apparent in figure 15(a). The thick boundary layer can cause a stall flutter, at the blade tips. Vibrating motion of the blade tips would cause the tip stall to appear and disappear at the natural blade vibration frequency. Stall flutter, discussed in more detail by Pearson (ref. 5), may account for the high blade stress levels at 8200 rpm.

Some additional follow-on studies, using a small model in a smoke stream tunnel, have aided in the understanding of the causes of the aforementioned stresses. At angles of attack above 90°, the inlet capture stream tube expands as airspeed is lowered, until a progressively greater amount of turbulent, stagnant air is drawn into the engine from the nacelle wake. The boundary layer from the entire exterior nacelle circumference is also drawn

into the engine, especially as airspeed decreases. This flow pattern is illustrated in figure 16.

The existence of a critical forward velocity (roughly 30 m/s) for this EO 3 vibration is illustrated in figure 17. The nacelle wake is apparently no longer ingested into the inlet beyond this forward velocity, and the EO 3 stress level decreases with increasing free-stream velocity. Note that EO 4 and EO 5 (lip separation related) stress does not decline with increasing airspeed since the lip flow remains separated over this range in free-stream velocity. Inlets for conventional takoff airplanes should also encounter nacelle wake ingestion during strong quartering tailwinds while on the ground.

General Stress Amplitude

Regardless of the type of excitation, blade stress remained generally below safe limits during testing, despite the high amplitude peaks that occurred at resonant speeds. Predictions of external conditions of airspeed and angle of attack that can cause limit blade stress will now be discussed. The data shown thus far indicate that dangerous blade vibrations occur only at resonant speeds, and that these are limited to EO 3 to 5, and possible 6 in decreasing severity. AT EO's above 6 (3800 rpm and below), stress was never dangerous, and resonant speeds were difficult to identify. The following discussion, therefore, is limited to EO resonant speeds 3 to 6, first bending mode only.

The amplitude of the stress peaks at each engine order resonant speed is plotted against angle of attack at various fixed free-stream velocities in figure 18. In general, at a fixed resonant mechanical speed the stress remained low until an angle of attack was reached that corresponded to the onset of inlet diffuser separation. Stress then rose rapidly as the inlet flow separation point approached the lip. At 3800 rpm (EO 6), (fig. 18(d)) stress leveled off at a moderate value after lip separation, so limit stress was not reached at this fan rotational speed. At the other speeds (EO 3 to 5), lip separation could be expected to produce blade stress levels greater than the limit. This trend permitted an extrapolation to the airspeed and angle of attack conditions at which the stress limit would occur. The extrapolations are shown as dashed lines in figures 18(a) to (c). These extrapolated values of airspeed and angle of attack where limit stresses would occur are then shown in figure 19, along with a typical operating envelope for the nacelle on a tilt-nacelle aircraft. All stress limitations were outside this particular envelope; and EO 3 was limiting at low airspeed and EO 5 was limiting at the higher airspeeds.

The angle of attack at which blade stress began to rise is taken from figure 18 and plotted against N/V_0 in figure 20. This angle of attack is assumed to correspond, as discussed previously, to the start of flow separation at the downstream end of the inlet diffuser. The parameter N/V_0 was chosen because of its similarity to the ratio of inlet throat velocity to free-stream velocity which is used in references 1 and 2 to generalize the inlet flow separation characteristics. The parameter N/V_0, or equivalent, is necessary to predict blade stress at airspeeds other than the particular ones tested.

Figure 20 is similar, if not identical, to aerodynamic flow separation curves for this inlet (refs. 1 and 2) and illustrates the expected close relationship between inlet aerodynamics and fan-blade vibration. Operation below the curve is considered completely free of significant blade vibra-

tion, with one qualification: at low speeds, the angle of attack must be less than 90° to avoid the nacelle wake ingestion problem.

SUMMARY OF RESULTS

A model tilt-nacelle with a 51 cm diameter fan was tested in the Lewis 9- by 15-Ft Wind Tunnel to determine the effects of inlet flow conditions on fan blade stress. The following results were obtained:

1. The fan-blade first flatwise bending was the only vibration mode excited. This observation was unexpected and may be unique to the particular blade design that was used.

2. Resonant peaks in the fan-blade stresses occurred only at integral engine orders. Between resonant speeds, all tested distortion conditions produced very low blade stress. The potentially dangerous blade vibrations that occurred at integral engine orders were related to two causes:

   a. At the higher tested free-stream velocities, inlet flow separation, especially at the lip, produced high blade stress.

   b. At lower free-stream velocities, and at angles of attack over 90°, high stresses occurred, apparently due to nacelle wake ingestion. These stresses are attributed to stall flutter at the blade tips.

3. Blade vibration, even at low stress levels, can be used as an extremely sensitive indication of flow conditions within the inlet.

APPENDIX

METHOD OF DETERMINING ALLOWABLE STRESS

The observed or "scope" limits were determined by the General Electric Company using a combined experimental and analytical method. A brief summary of the steps involved follows:

1. Determine steady-state blade loading at maximum design conditions. The determinations were made via computer program except near the root, where experimental loads were applied to determine stress concentration factors.

2. The blade was vibrated in the laboratory while fitted with more than 40 strain gages. Eight natural frequencies were determined. Critical gage locations were noted at each frequency, where the combination of vibratory and steady stress would be most likely to initiate a fatigue crack. The above results were analytically modified to account for centrifugal effects expected during operation.

3. One gage location was chosen for operational use. At each of the eight natural frequencies, a ratio of stress at the operational location (stress g) divided by stress at the critical point (stress c) was determined.

4. A stress allowable (stress e) was determined from a titanium alloy Goodman diagram, based on standard spectrum statistical test results.

5. Safety factors were added for blade-to-blade variation ($K_1 = 1.3$), electronic inaccuracy ($k_2 = 1.05$), and possible stress concentration at the blade root ($K_3 = 1.2$). Since double amplitude is used customarily as a scope limit, the final limit for safe operation is given as

$$\text{scope limit} = \frac{2\,\frac{(\text{stress g})}{(\text{stress c})}\,\text{stress e}}{K_1 K_2 K_3}$$

6. Although the scope limits apply only to 100-percent design speed at the design pressure ratio and blade angle, they were used as operational limits throughout the entire range of simulator operation. This was done for simplicity and for an additional safety factor at lower fan speeds.

7. The final operational (scope) limits for the four lowest natural frequencies were:

First flatwise bending (400 Hz) 35000 psi (double amplitude)
First axial (edgewise) (840 Hz) 11500 psi
First torsion (1200 Hz) 23500 psi
Second flatwise bending (1850 Hz) 25000 psi

REFERENCES

1. Syberg, J.; and Koncsek, J.: Low Speed Tests of a Fixed Geometry Inlet for a Tilt-Nacelle V/STOL Airplane. (D180-20276-1, Boeing Co.; NASA Contract NAS2-9215.) NASA CR-151922, 1977.

2. Koncsek, J. L.; and Shaw, R. J.: Operating Characteristics of an Inlet Model Tested with a 0.5M Powered Fan at High Angles of Attack. (D180-20798-1, Boeing Co.; NASA Contract NAS3-20597.) NASA Cr-135270, 1977.

3. Lewis, George W. Jr.; and Tysl, Edward R.: Overall and Blade-Element Performance of a 1.20-Pressure-Ratio Fan Stage at Design Blade Setting Angle. NASA TM X 3101, Sept., 1974.

4. Yuska, Joseph A.; Diedrich, James H.: and Clough, Nester: Lewis 9- by 15-Ft V/STOL Wind Tunnel. NASA TM X-2305, 1971.

5. Pearson, H.: The Aerodynamics of Compressor Blade Vibration. Proceedings of the Fourth Anglo-American Aeronautical Conference, Aeronautical Society, 1953, pp. 127-162.

6. Danforth, C.E.: Distortion Induced Vibration in Fan and Compressor Blades. AIAA Paper 74-232, Feb., 1974.

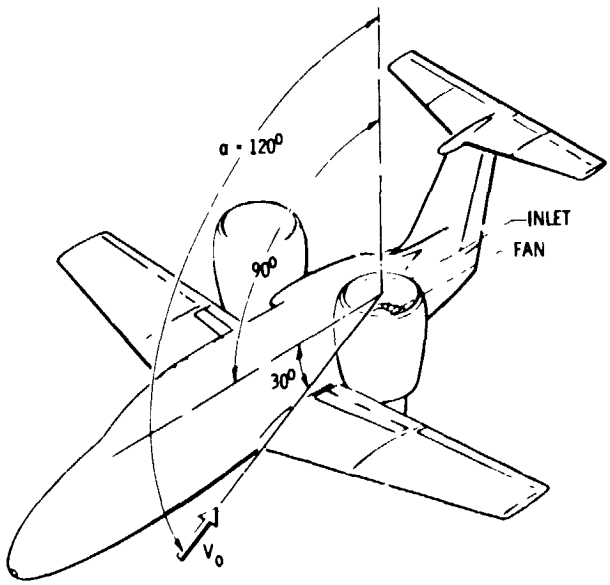

Figure 1. - Tilt nacelle VI STOL aircraft.

Figure 2. - The 51-cm-diam fan rotor used for blade stress testing.

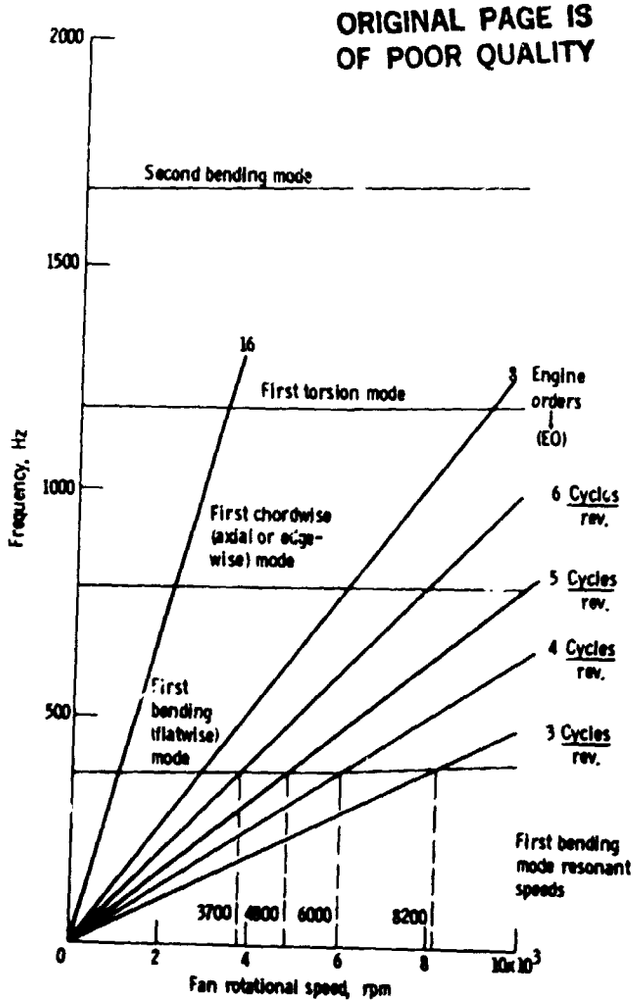

Figure 3. - Campbell diagram for fan blades.

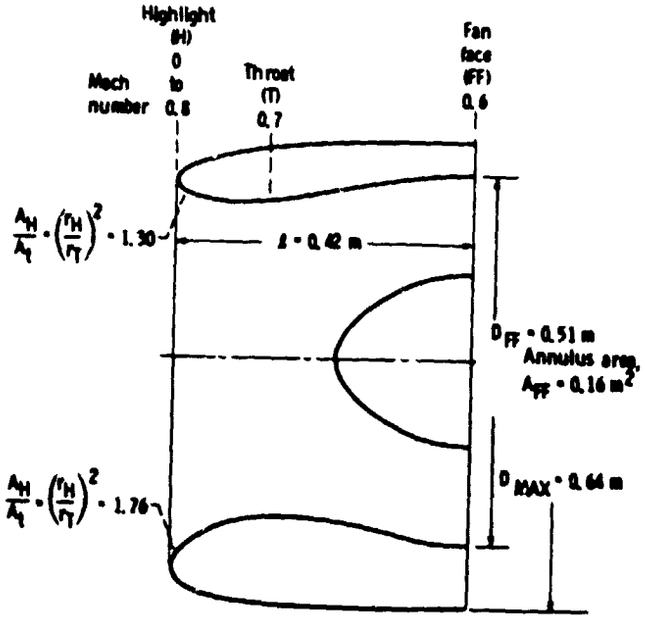

Figure 4. - Sketch of asymmetric inlet.

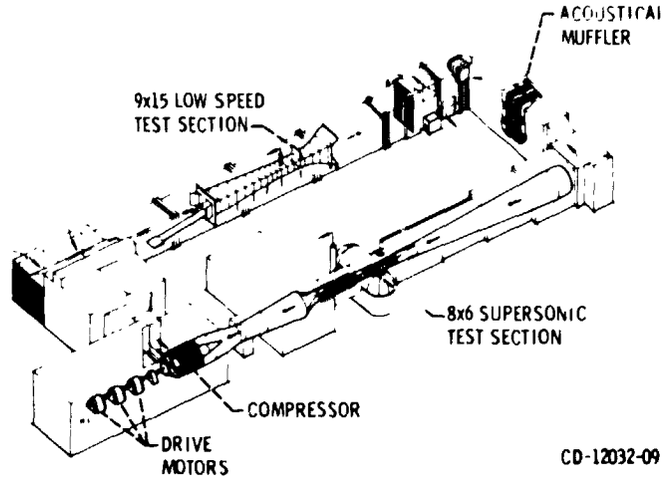

Figure 5. - The NASA Lewis 8 by 6 Supersonic and 9 by 15 Low Speed Wind Tunnels.

Figure 6. - Model fan installed in the 9 by 15 wind tunnel.

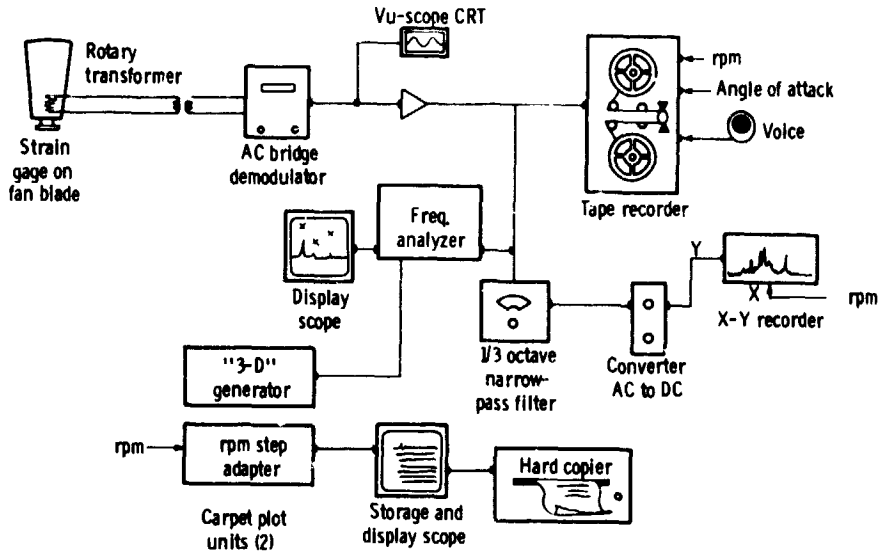

Figure 7. - Blade strain data acquisition, recording, and display system.

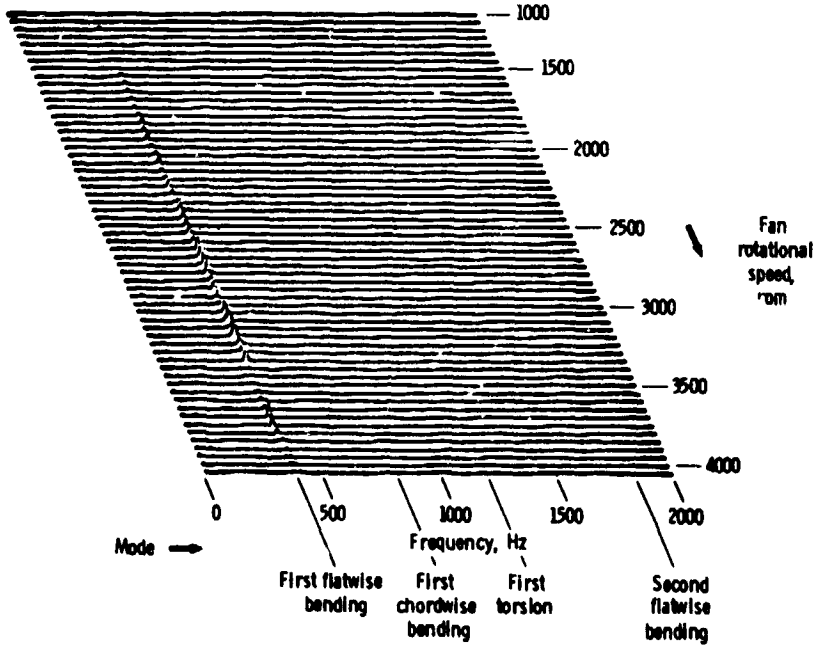

Figure 8. - Typical three-dimensional spectral plot (carpet plot).

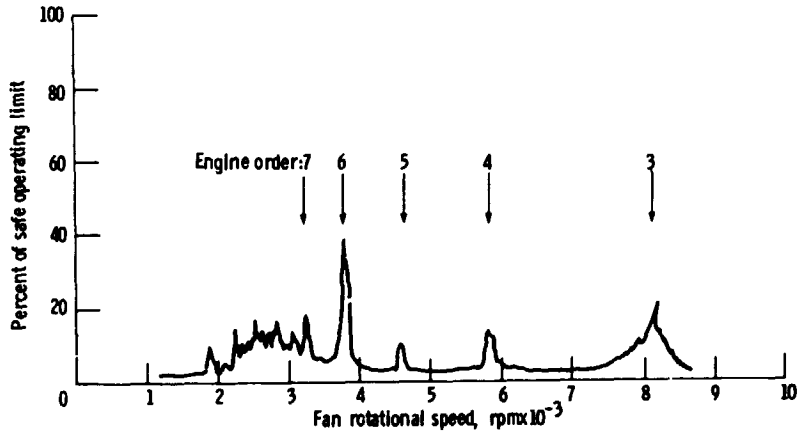

Figure 9. - Typical fan blade vibratory stress variation (first flatwise bending mode).

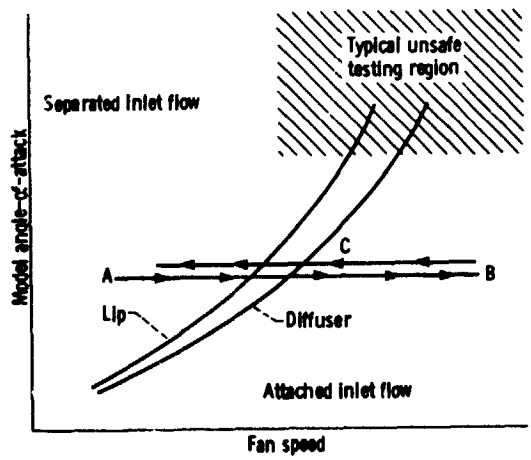

Figure 10. - Data acquisition procedure.

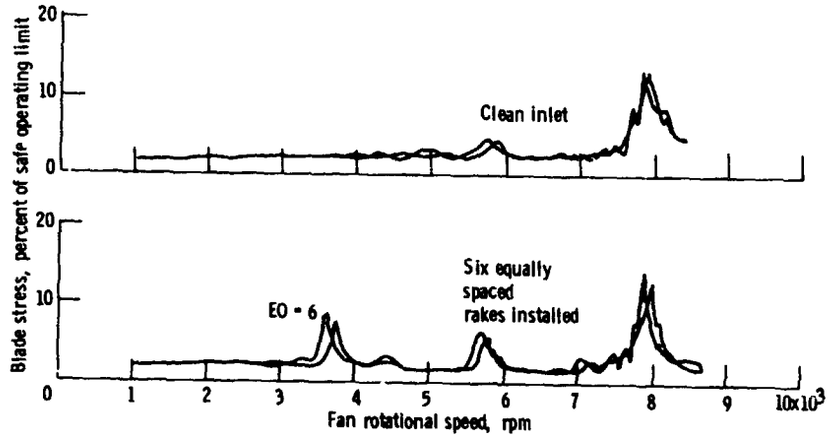

Figure 11. - Blade stress X-Y plots showing the effect of instrumentation rakes just upstream of the fan.

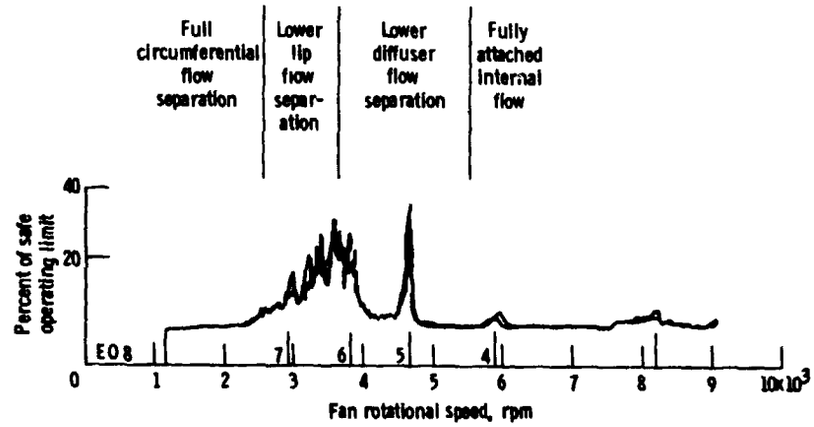

Figure 12. - Typical blade stress data, V_0 = 39 m/sec; $\alpha = 90^0$.

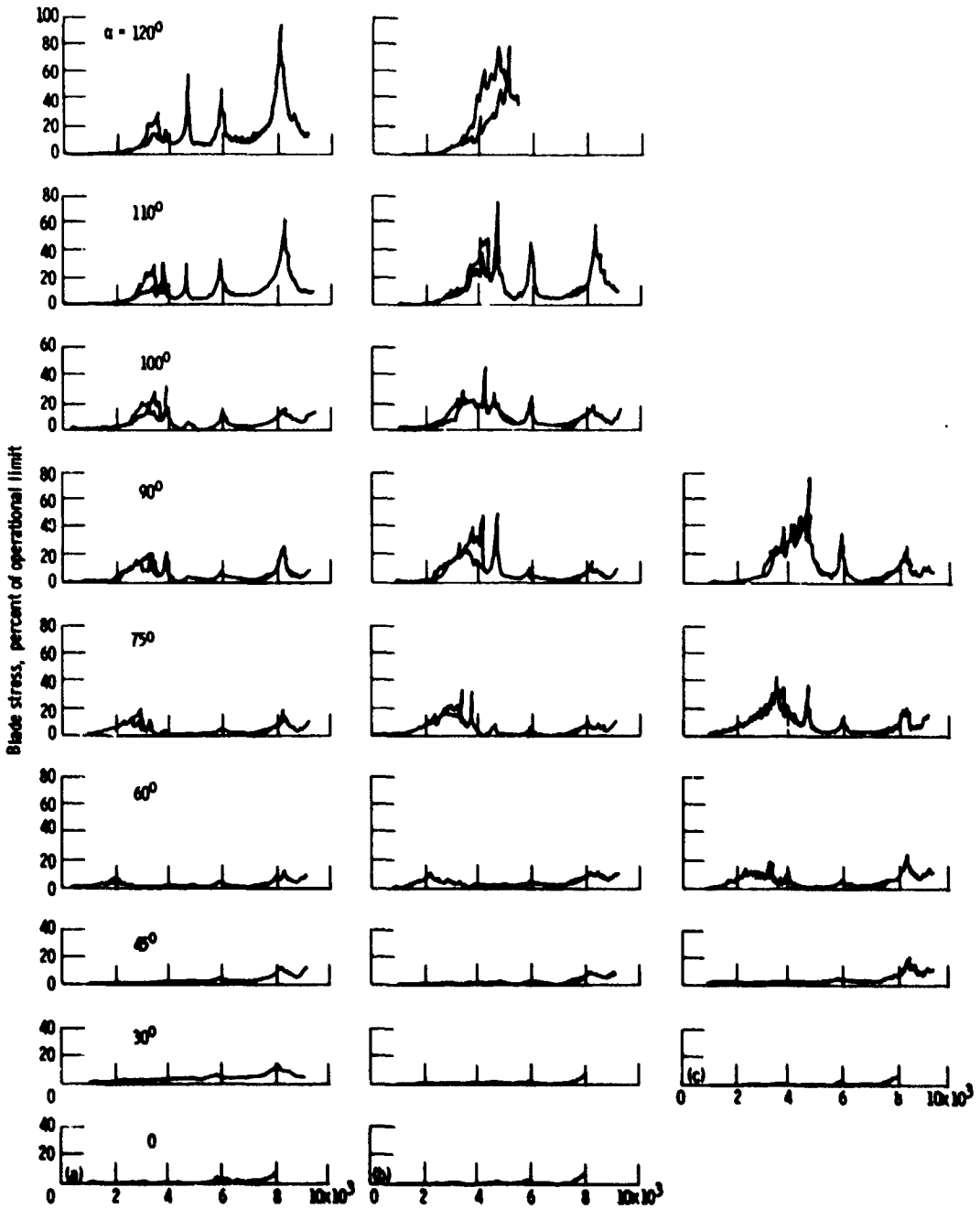

(a) Free-stream velocity, 30.8 m/sec.
(b) Free-stream velocity, 38.6 m/sec.
(c) Free-stream velocity, 46.3 m/sec.

Figure 13. - Composite blade stress data.

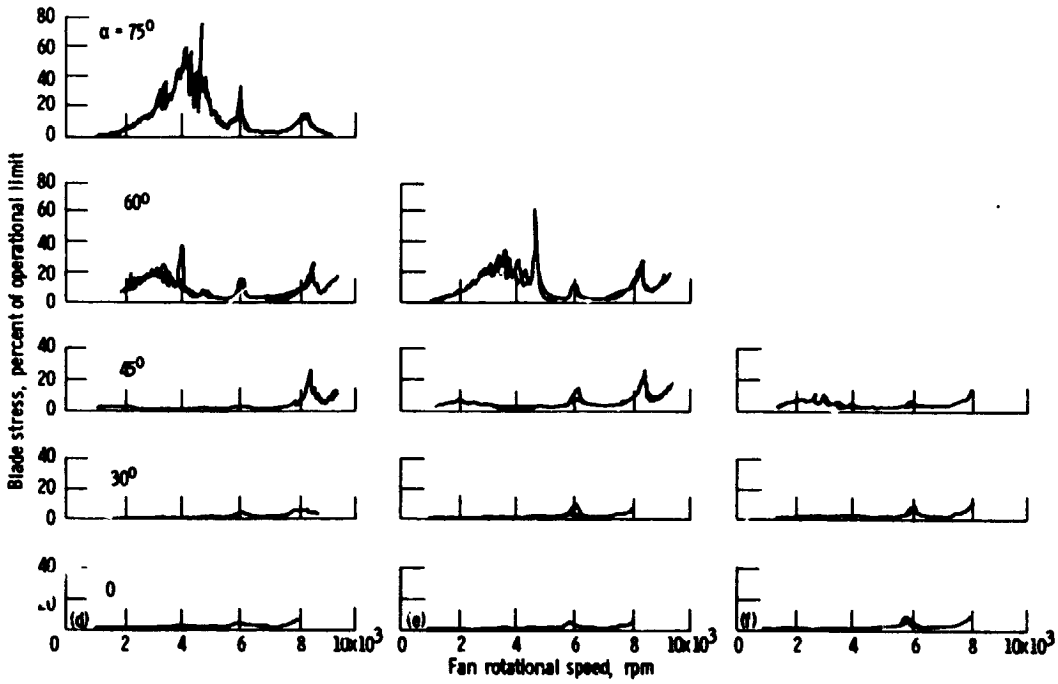

(d) Free-stream velocity, 54 m/sec.
(e) Free-stream velocity, 64.3 m/sec.
(f) Free-stream velocity, 72.0 m/sec.

Figure 13. - Concluded.

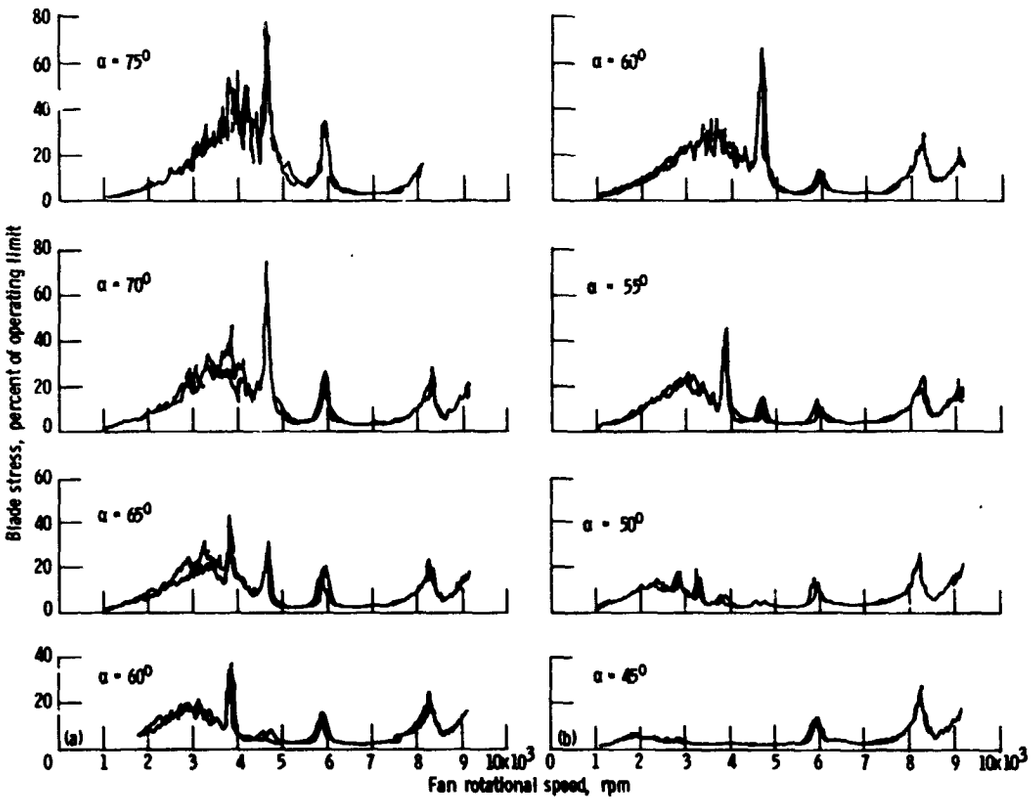

(a) Free-stream velocity, 54 m/sec.

(b) Free-stream velocity, 64.3 m/sec.

Figure 14. - Blade stress data taken at 5° increments of angle of attack.

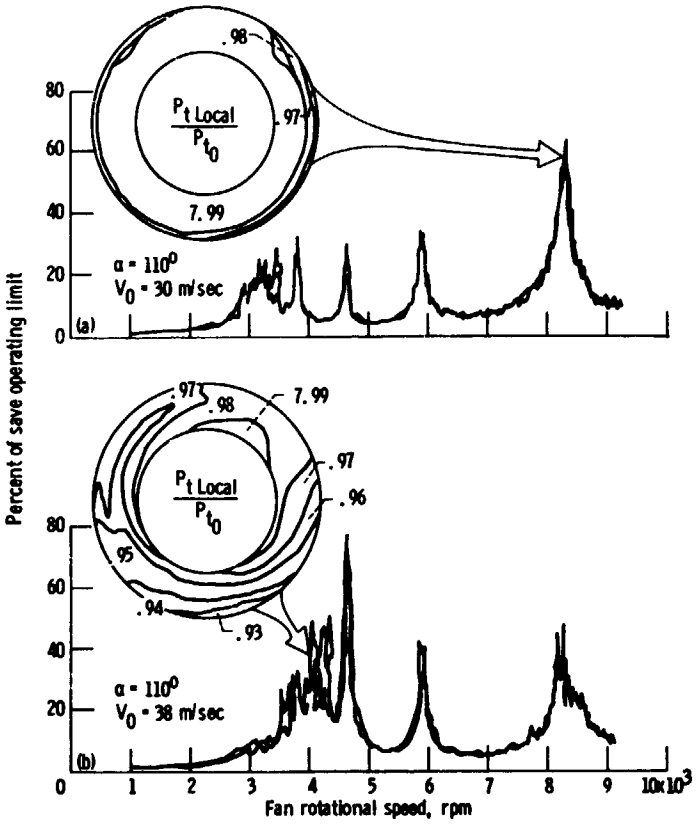

(a) Distortion due to thick boundary layer.

(b) Distortion due to flow separation.

Figure 15. - Total pressure distortion patterns associated with fan blade vibration.

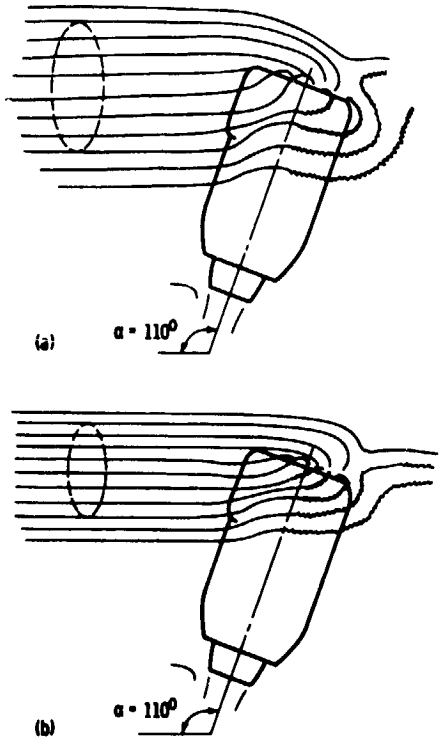

(a) Larger capture stream tube; velocity, 30 m/sec. Larger portion of turbulent nacelle wake is ingested, causing high blade stress.

(b) Smaller capture stream tube; velocity, 38 m/sec. Smaller portion of nacelle wake is ingested causing only moderate blade stress.

Figure 16. - Sketches of exterior streamlines based on smoke tunnel observations. Nacelle wakes are very unsteady.

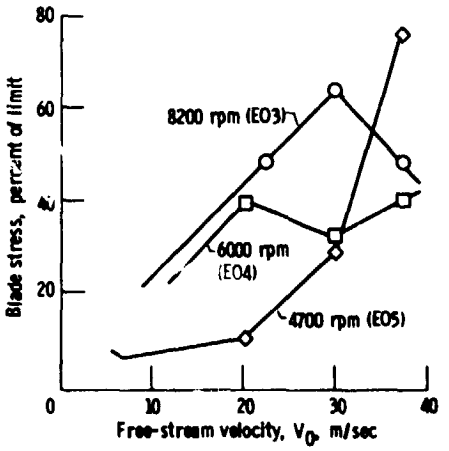

Figure 17. - Peak resonant blade stress at constant angle of attack (110°) and constant rpm.

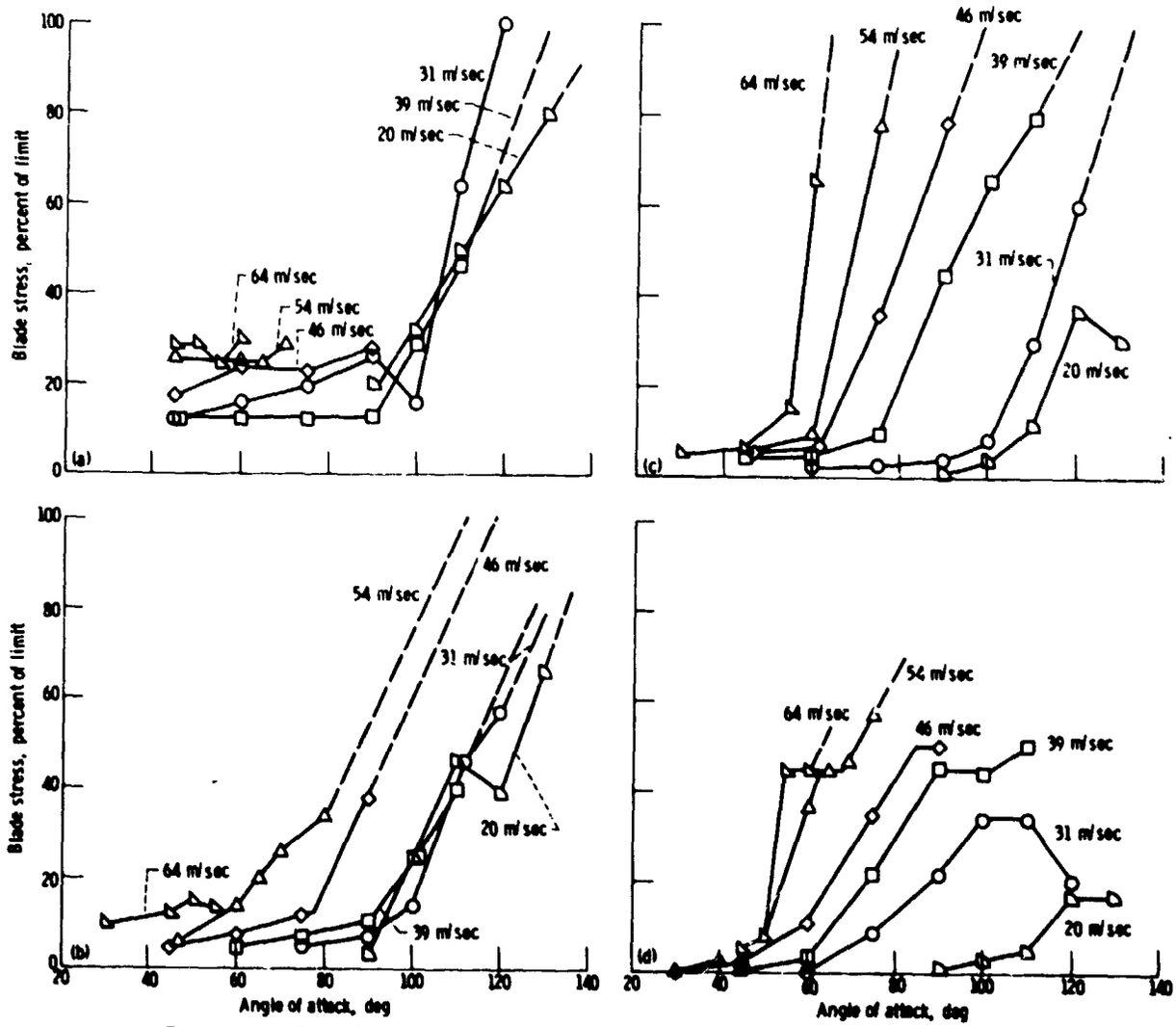

(a) Three per revolution (EO3) stress (8200 rpm).
(b) Four per revolution (EO4) stress (6000 rpm).
(c) Five per revolution (EO5) stress (4800 rpm).
(d) Six per revolution (EO6) stress (3800 rpm).

Figure 18. - Variation of peak blade stress versus angle of attack at various airspeeds.

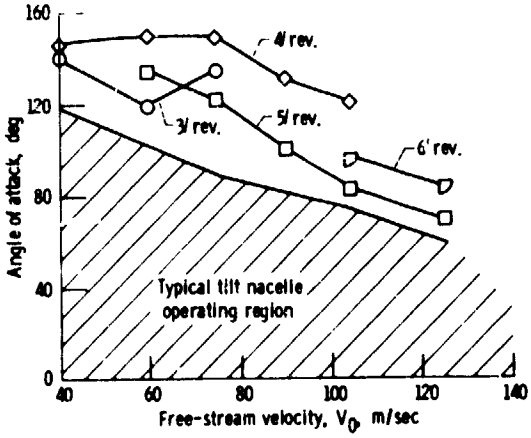

Figure 19. - Fan blade stress limits and aircraft operating requirements.

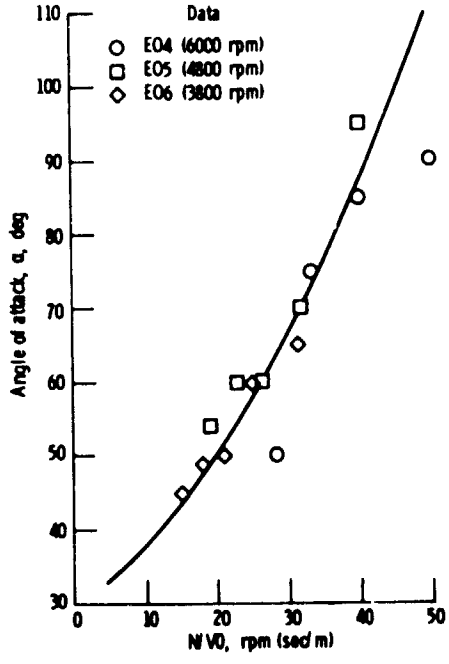

Figure 20. - Angle of attack at which blade stress rises, plotted against N/V0.